Ab initio study of the phase stability in paramagnetic duplex steel alloys

H. Pitkänen,[1,*] M. Alatalo,[1] A. Puisto,[2] M. Ropo,[3,4,5] K. Kokko,[3] M. P. J. Punkkinen,[3] P. Olsson,[6] B. Johansson,[5,7] S. Hertzman,[8] and L. Vitos[5,7,9]

[1]*Department of Mathematics and Physics, Lappeenranta University of Technology, P.O. Box 20, FIN-53851 Lappeenranta, Finland*

[2]*Department of Applied Physics, Helsinki University of Technology, P.O. Box 1100, FI-02015 HUT Espoo, Finland*

[3]*Department of Physics and Astronomy, University of Turku, FIN-20014 Turku, Finland*

[4]*Department of Information Technology, Åbo Akademi, Fin-20500 Turku, Finland*

[5]*Department of Materials Science and Engineering, Applied Materials Physics, Royal Institute of Technology, Stockholm SE-100 44, Sweden*

[6]*Department of Materials and Mechanics of Components, EDF R&D, F-77250 Moret-sur-Loing, France*

[7]*Department of Physics and Materials Science, Division for Materials Theory, Uppsala University, SE-75121 Uppsala, Sweden*

[8]*Department of Materials Science and Engineering, Outokumpu Stainless Research Foundation, Royal Institute of Technology, Stockholm SE-100 44, Sweden*

[9]*Research Institute for Solid State Physics and Optics, P.O. Box 49, Budapest H-1525, Hungary*

(Received 26 September 2008; revised manuscript received 26 November 2008; published 15 January 2009)

Duplex stainless steels have many superior properties compared to conventional steels, this being mainly due to their microstructure containing approximately equal amount of ferrite and austenite phases formed by iron, chromium (or Cr equivalent), and nickel (or Ni equivalent). Using computational methods based on first-principles theories, the phase stability of paramagnetic $Fe_{1-c-n}Cr_cNi_n$ alloys ($0.12 \leq c \leq 0.32$ and $0.04 \leq n \leq 0.32$) at high temperatures ($\gtrsim 1000$ K) is addressed. It is shown that the stabilization of the ferrite-austenite two-phase field in duplex steels is a result of complex interplay of several competing phenomena. Taking into account only the formation energies yields a complete phase separation, strongly overestimating the two-phase region. The formation energies are calculated to be lower for the austenite than for the ferrite, meaning that the configurational entropy has a more significant impact on the stability field of the austenitic phase. The magnetic and vibrational free energies have opposite effects on the phase stability. Namely, the magnetic entropy favors the ferrite phase, whereas the vibrational free energy stabilizes the austenite phase. Combining the formation energies with the magnetic, vibrational, and configurational free energies, a region of coexistence between the two phases is obtained, in line with former thermodynamic assessments as well as with experimental observations.

DOI: 10.1103/PhysRevB.79.024108 PACS number(s): 64.30.Ef, 71.15.Nc, 75.50.Bb, 81.05.Zx

I. INTRODUCTION

Stainless steels form the largest family of maintenance-free and safe engineering materials. The main stainless groups are austenitic and ferritic steels.[1] Today a third important group is developing around the so-called duplex grades. These steels offer a unique combination of outstanding mechanical performance and appropriate corrosion resistance and present promising alternative materials for various technological applications. Furthermore, since duplex steels usually have twice the mechanical strength of conventional steels, the material cost may significantly be reduced with this class of materials.

Figure 1 is a schematic representation of the Schäffler phase diagram for stainless steels.[1] The diagram describes the empirically determined weld microstructures and corresponds to the situation at around 1300 K. The phases are shown as a function of Ni (Ni equivalent: Ni, C, N, Mn, etc.) and Cr (Cr equivalent: Cr, Mo, Si, Nb, V, Al, etc.). Ferrites are formed in low-Ni and high-Cr alloys; the austenitic phase is stable in high-Ni alloys, whereas low-Ni and low-Cr alloys form the martensitic phase. The duplex grades are located within the two-phase field between the ferrite and austenite phases, containing minima of 4–6 wt % Ni and 22–24 wt % Cr. Recently, researchers designed low-Ni du-

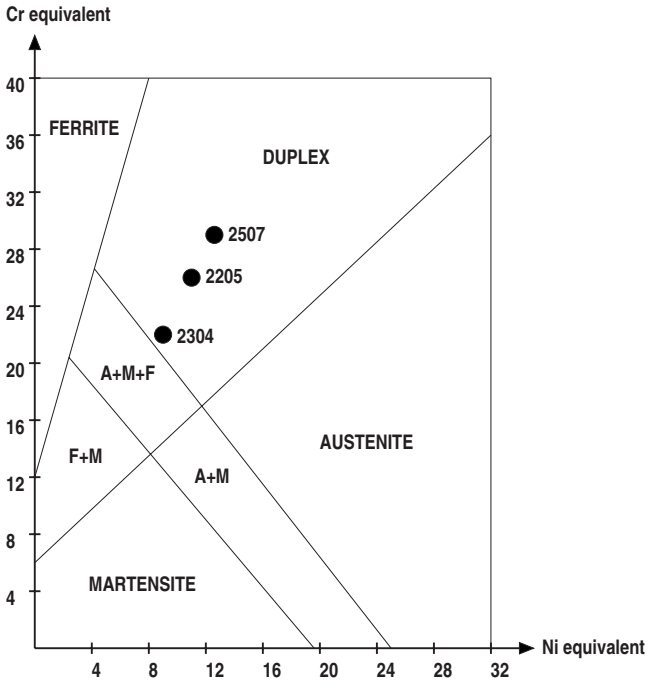

FIG. 1. Schematic of the Schäffler diagram. Concentrations are given in wt %. The numbers represent a few commercially available duplex steel alloys.

plex stainless steels for construction purposes,[2] which have now become a world-leading duplex grade. The new duplex steels encompass approximately 22% Cr, 5% Mn, and 1%–2% Ni, plus small amounts of Si, Mo, Cu, N, and C.

The specific properties of duplex steels are to a large extent determined by the austenite-ferrite phase ratio. At normal conditions, most of the commercial grades have microstructure containing approximately equal volumes of ferrite and austenite. This balance can, however, be destroyed in the so-called heat-affected zones (e.g., during welding), which is detrimental for the chemical and mechanical properties. Low austenite reformation, for instance, may lead to increased susceptibility to pitting corrosion. Therefore, understanding the thermodynamics of the Fe-based alloys with chemical compositions between ferrite and austenite phases is of fundamental importance for an efficient control of the properties of duplex steels.

Attempts based on experiment as well as on semiempirical approaches have been made to describe the phase equilibrium and austenite reformation in duplex stainless steels.[3–7] However, due to the complexity of the problem, so far very little is known about the behavior and formation of duplex steels at atomic scale. The aim of the present study is to reduce this deficiency by investigating the thermodynamics of the duplex steels using first-principles quantum-mechanical theories. To this end, we perform a number of *ab initio* electronic structure and total-energy calculations for the austenitic and ferritic steels and study the phase stability as a function of chemical composition.

To simplify the above task and make it manageable by the available theories and methods, we introduce several approximations. We consider homogeneous Fe-Cr-Ni alloys, without interstitial elements and without precipitates. In particular, in the ferrite phase we neglect the intermetallic sigma phase (σ) and the Cr-rich spinodal (α') precipitation.[8,9] We model the two alloy phases by their main building blocks. Namely, the austenitic steel is represented by a face-centered-cubic (fcc) alloy and the ferrite steel by a body-centered-cubic (bcc) alloy. The short-range order and local relaxation effects are omitted and both phases are treated as substitutional random alloys. The martensite phase is not considered here, and the energetics associated with phase boundaries are also neglected.

At low temperature, the magnetic structure of Fe-Cr-Ni ternary alloys can be antiferromagnetic, spin glass, or ferromagnetic, depending on Ni and Cr content.[10] At room temperature, the austenitic phase is paramagnetic, whereas the magnetic transition temperature for the ferritic phase is close to the magnetic transition temperature of pure Fe. Accordingly, at service conditions the magnetic structure of duplex steels is expected to be ferromagnetic in the ferrite region and paramagnetic in the austenite region. This picture has been confirmed by the recent magnetic force microscopy measurements performed on Fe23Cr5Ni3Mo duplex steels.[11] In the present study, however, in order to be able to treat the magnetic free energy in both fcc and bcc phases on an equal footing, we limit ourselves to the high-temperature paramagnetic phase, i.e., to temperatures above 1000 K.

The Schäffler diagram (Fig. 1) illustrates the importance of the alloying elements in the phase balance in duplex steel grades. It is well known that interstitial carbon and nitrogen have a strong effect on the phase stability of austenitic stainless steels. However, modeling the effect of interstitials from first-principles theory is very cumbersome especially in the case of a chemically and magnetically disordered matrix. On the other hand, the major and most important alloying elements for duplex steels are the Cr and Ni and the duplex grades are developed around the two elements and the phase constitution determined by them. Hence, it is of utmost importance to be able to model the ternary Fe-Cr-Ni system in order to understand the duplex grades. Accordingly, in the present work all austenite stabilizers (the Ni-equivalent components) are represented by Ni. Because of that, we extend our theoretical study beyond the usual Ni concentrations in commercial grades and consider alloys containing from 4% up to 32% substitutional Ni. Similarly, we set the concentration range for Cr between 12% (given by the stainless requirement[12]) and 32%. According to the binary phase diagram of Fe-Cr and Fe-Ni, at temperatures considered here ($T \geq 1000$ K), about 20%–30% Cr can be dissolved in bcc Fe (α-Fe), and there is no solubility limit between Ni and fcc Fe (γ-Fe). The latter is, however, stable only above 1185 K. At 1000 K, about 10% Ni is needed to stabilize the γ phase.

As a reference for our theoretical results for the Fe-Cr-Ni ternary system, we use the phase diagram obtained at 1123 K for the Fe-Cr-Ni systems using thermodynamic assessment[3] based on subregular solution model.[13,14] In the following we refer to this semiempirical graph as the TA1123 diagram. We emphasize that the TA1123 diagram reproduces very well the experimental phase boundaries by Eriksson[3,15] and thus can be considered as accurate as the experimental data.

The paper is organized as follows. In Sec. II, we briefly introduce the method used in our calculations and give details about how the Gibbs energy is calculated. In Sec. III, we demonstrate our results for the main energy components using the quasibinary system $Fe_{0.84-n}Cr_{0.16}Ni_n$ and give the theoretical phase diagram for $Fe_{1-c-n}Cr_cNi_n$ obtained at 1000 K. The paper ends with conclusions.

II. METHODOLOGY

A. Modeling the paramagnetic Fe-Cr-Ni alloys

For an adequate simulation of paramagnetic alloy steels both the chemical and magnetic disorders should be treated simultaneously.[16] In the present application, we model the paramagnetic ternary $Fe_{1-c-n}Cr_cNi_n$ system by an alloy with randomly distributed chemical species and local magnetic moments, i.e., by a four component random $Fe^{\uparrow}_{(1-c-n)/2}Fe^{\downarrow}_{(1-c-n)/2}Cr_cNi_n$ alloy. Here the arrows represent the two magnetic moments oriented up ($\uparrow$) and down ($\downarrow$). This disordered local-moment (DLM) approach accurately describes the effect of loss of the net magnetic moment above the transition temperature.[17] Note that the small local magnetic moments on Cr and Ni sites, present at high temperature (longitudinal spin fluctuations),[18] have been neglected in the above approximation. Their contribution to the total energy and thus to the fcc-bcc phase stability remains to be investigated. In magnetic systems magnetovolume effects[19,20] can make the theoretical assessment of the equa-

tion of state as a function of composition very difficult. However, in Fe-Cr-Ni alloys, for the compositional range considered here, no volume-induced magnetic transitions have been observed in the DLM state.

B. Computational method

The stability field of the fcc and bcc phases of Fe-Cr-Ni alloys is established by comparing the corresponding Gibbs free energies calculated as a function of chemical composition and temperature. The Gibbs free energy, in turn, is derived from the total energy plus the temperature-dependent terms. The most straightforward way to compute the total energy of a random alloy is to consider a huge supercell with randomly distributed solute atoms. However, in the present case we are facing a four component alloy, and therefore an accurate description of its energetics as a function of concentration would require enormously large and numerous supercells. Here, we resolve this difficulty by employing the coherent potential approximation (CPA).[21] Within the CPA, the alloy components are embedded in an effective medium, which is constructed in such a way that it represents, on the average, the scattering properties of the alloy. In this way, the original alloy problem reduces to the Schrödinger equation for the effective medium plus the real-space Dyson equations written for each single impurity. In the present application, we adopt the CPA implemented within the frameworks of the exact muffin-tin orbital (EMTO) method.[16,22]

The EMTO method is an improved screened Korringa-Kohn-Rostoker method,[23] where the one-electron potential is represented by large overlapping muffin-tin potential spheres. By using overlapping spheres, one describes more accurately the crystal potential when compared to the conventional nonoverlapping muffin-tin approach.[24–26] The EMTO approach has been applied successfully in the theoretical study of the elastic constants and phase stability of random Fe-based alloys,[18,27–31] simple and transition-metal alloys,[32–35] and Hume-Rothery systems,[22,36,37] as well as the crystal structure of complex oxides.[38–41] Therefore, the EMTO method ensures the accuracy and efficiency needed for the calculations of the total energy for different crystallographic phases of Fe-Cr-Ni random alloys.

All the calculations from the present work were carried out using the generalized-gradient approximation[42] for the exchange-correlation density functional. The EMTO basis set included s, p, d, and f orbitals. The one-electron equations were solved within the scalar-relativistic and frozen-core approximation. For each composition and crystal lattice, the EMTO Green's function was calculated self-consistently for 16 complex energy points distributed exponentially on a semicircular contour, which included states within 1 Ry below the Fermi level. In the one-center expansion of the full charge density, we adopted an l-cutoff of 10 and the total energy was calculated using the full charge density technique.[16,25]

C. Thermodynamic model

We approximate the Gibbs free energy of the $Fe_{1-c-n}Cr_cNi_n$ random alloy by

$$G^{\mathrm{str}}(c,n) = H^{\mathrm{str}}(c,n) - T[S_{\mathrm{conf}}(c,n) + S^{\mathrm{str}}_{\mathrm{mag}}(c,n)] + F^{\mathrm{str}}_{\mathrm{vib}}(c,n), \tag{1}$$

where str stands for fcc or bcc and T is the temperature. H is the enthalpy, S_{conf} is the configurational entropy, S_{mag} is the magnetic entropy, and F_{vib} is the vibrational free energy. In the above expression, the electronic entropy has been omitted. However, our previous studies[18,30] show that in the paramagnetic Fe-Cr-Ni system, the Fermi distribution gives a negligible contribution compared to other entropy terms.

At static conditions (T=0 K), the Gibbs free energy $G^{\mathrm{str}}(c,n)$ reduces to the internal energy $E^{\mathrm{str}}(c,n)$, which is obtained directly from the self-consistent EMTO calculations carried out at the theoretical equilibrium volumes $V_0(c,n)$ corresponding to concentrations c and n. At nonzero temperature, we take into account the explicit temperature-dependent terms on the right-hand side of Eq. (1). For the configuration and magnetic entropies we use the mean-field expressions,

$$S_{\mathrm{conf}}(c,n) = -k_B[(1-c-n)\ln(1-c-n) + c\,\ln(c) + n\,\ln(n)] \tag{2}$$

and

$$S^{\mathrm{str}}_{\mathrm{mag}}(c,n) = -k_B(1-c-n)\ln[1+\mu^{\mathrm{str}}_{\mathrm{Fe}}(c,n)], \tag{3}$$

valid for a fully disordered state (k_B is the Boltzmann constant). Although the chemical and magnetic short-range order would have a significant effect on $S_{\mathrm{conf}}(c,n)$ and $S_{\mathrm{mag}}(c,n)$, we expect that at temperatures considered here the ordering effects are small and thus the above expressions correctly describe the configurational and magnetic entropy contributions to the free energy.

The local magnetic moments on the Fe atoms, $\mu^{\mathrm{str}}_{\mathrm{Fe}}(c,n)$, are obtained from EMTO calculations, and they depend on the crystal structure and chemical composition. To go beyond the present approximation for the magnetic free energy of paramagnetic Fe-Cr-Ni alloys, one should also consider the temperature dependence of the local magnetic moments on Fe as well as on Cr and Ni sites. This would require a proper description of the high-temperature magnetic fluctuations,[43] taking into account the complex magnetic and magnetoelastic interactions.[18,30,44] This is, however, beyond the reach of the present research.

Today, a direct phonon calculation for the chemically and magnetically disordered Fe-Cr-Ni system is not feasible. Therefore, in this work the vibrational free energy is calculated within the Debye model according to

$$F^{\mathrm{str}}_{\mathrm{vib}}(c,n) = -k_BT\left[\frac{3}{(\Theta_D/T)^3}\int_0^{\Theta_D/T}\frac{x^3}{e^x-1}dx - 3\,\ln(1-e^{-\Theta_D/T}) - \frac{9\Theta_D}{8T}\right], \tag{4}$$

where Θ_D is the Debye temperature. Note that Θ_D depends on the crystal structure, composition, and temperature. Within the simplest Debye approximation, the elastic Debye temperature is obtained from the equilibrium atomic radius

(Wigner-Seitz radius) w, atomic mass M, Poisson's ratio ν, and bulk modulus B as

$$\Theta_D = \frac{h}{k_B}\left(\frac{4\pi}{3}\right)^{-1/6} F(\nu)\left(\frac{wB}{M}\right)^{1/2}, \quad (5)$$

where h is the Planck constant. Explicit expression for the function $F(\nu)$ is given in Ref. 45. In the present application, Poisson's ratio was assumed to be 1/3, i.e., $F(\nu)=0.69$. The calculated equilibrium atomic radii of paramagnetic Fe-Cr-Ni alloys exhibit a weak composition dependence on the concentration range considered here: they vary between 2.660 and 2.668 bohr for fcc and 2.672 and 2.682 bohr for bcc. On the other hand, the bulk moduli vary within 140–180 GPa for fcc and 175–200 GPa for bcc. Therefore, the main concentration and structure dependence in Θ_D comes from the bulk modulus.

The phase stability of a ternary system is obtained from the common-tangent plane construction.[46] This is a rather cumbersome procedure in the case of complex energy surfaces. In order to be able to discuss the role of different energy contributions to the phase equilibria of Fe-Cr-Ni alloys, we first simplify the above two-dimensional problem to a one-dimensional problem. Namely, we regard the $Fe_{1-c-n}Cr_cNi_n$ alloy as a quasibinary system by assuming the Cr content constant ($c=c_0$). We denote the lowest and the highest Ni contents by α and β, respectively. In this way, we can adopt the common-tangent line technique[46] to find the two-phase field between the ferrite and austenite regions. Then the Gibbs free energy of formation for the crystal structure str is obtained as

$$\Delta G^{\mathrm{str}}(c_0,n) = G^{\mathrm{str}}(c_0,n) - (1-n)A - nB, \quad (6)$$

where A and B are the two reference energies. As standard states, we take the fcc phase at high-Ni end and the bcc phase at low-Ni end, with Gibbs energies $G^{\beta} \equiv G^{\mathrm{fcc}}(c_0,\beta)$ and $G^{\alpha} \equiv G^{\mathrm{bcc}}(c_0,\alpha)$, respectively. With this choice, we have

$$\Delta G^{\mathrm{str}}(c_0,n) = G^{\mathrm{str}}(c_0,n) - [(\alpha-n)G^{\beta} - (\beta-n)G^{\alpha}]/(\alpha-\beta). \quad (7)$$

This expression is used in Sec. III A to compute $\Delta G^{\mathrm{fcc}}(c_0,n)$ and $\Delta G^{\mathrm{bcc}}(c_0,n)$ as a function of n and to investigate the quasibinary phase diagram for $Fe_{1-c_0-n}Cr_{c_0}Ni_n$. In the actual calculations, we fix the Cr concentration to $c_0=0.16$ and take $\alpha=0.04$ and $\beta=0.32$.

For the ternary phase diagram, the Gibbs energy of formation for the crystal structure str is obtained as

$$\Delta G^{\mathrm{str}}(c,n) = G^{\mathrm{str}}(c,n) - (1-c-n)\mathcal{A} - c\mathcal{B} - n\mathcal{C}, \quad (8)$$

where the reference energies $\mathcal{A}$, $\mathcal{B}$, and $\mathcal{C}$ are obtained from the Gibbs energies of the standard states. We take as standard states the fcc phase at high-Ni and low-Cr corners [with Gibbs energy $G^{\mathrm{fcc}}(0.12,0.32)$] and the bcc phase at low-Ni and high-Cr corners [$G^{\mathrm{bcc}}(0.32,0.04)$] and at low-Ni and low-Cr corners [$G^{\mathrm{bcc}}(0.12,0.04)$]. Equation (8) is used in Sec. III B to compute $\Delta G^{\mathrm{fcc}}(c,n)$ and $\Delta G^{\mathrm{bcc}}(c,n)$ as a function of c ($0.12 \le c \le 0.32$) and n ($0.04 \le n \le 0.32$) on a grid of $\Delta c = \Delta n = 0.04$.

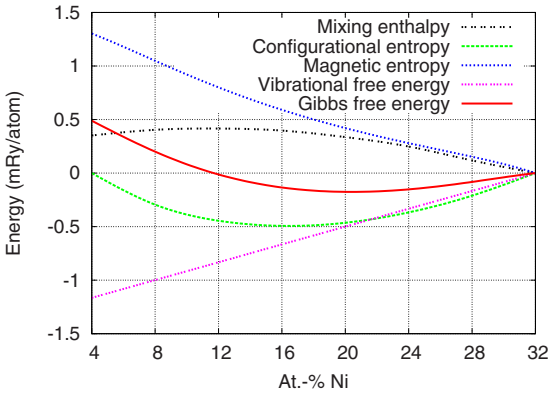

FIG. 2. (Color online) Calculated enthalpy and entropy contributions to the Gibbs free energy of formation for fcc $Fe_{0.84-n}Cr_{0.16}Ni_n$ plotted as a function of Ni content.

III. RESULTS AND DISCUSSION

A. Quasibinary $Fe_{0.84-n}Cr_{0.16}Ni_n$ system

Figures 2 and 3 show the enthalpy and entropy contributions to the Gibbs energies of formation at $T=1000$ K for fcc and bcc $Fe_{0.84-n}Cr_{0.16}Ni_n$ alloys as a function of Ni content. For both structures, the mixing enthalpy turns out to be positive, indicating the instability of the alloys at low temperature with respect to the present standard states, namely, bcc $Fe_{0.80}Cr_{0.16}Ni_{0.04}$ and fcc $Fe_{0.52}Cr_{0.16}Ni_{0.32}$. This result is in sharp contradiction to the TA1123 diagram obtained from thermodynamic assessment at 1123 K (Fig. 9 of Ref. 3). Namely, according to TA1123, the two-phase field for $Fe_{0.84-n}Cr_{0.16}Ni_n$ should extend up to $n \lesssim 0.03$, and for $n \gtrsim 0.03$ the alloy should crystallize in the austenite phase.

The mixing entropy [Eq. (2)] always favors the nonsegregated systems. However, since it is structure independent, its influence on the duplex region appears only via the particular shape of the mixing enthalpy. The situation is more interesting for the other two free-energy terms. The magnetic entropy is found to stabilize the bcc phase against the fcc phase. The calculated local magnetic moments are shown in Fig. 4 as a function of Ni content. The moments are significantly larger in the bcc structure than in the fcc one. In

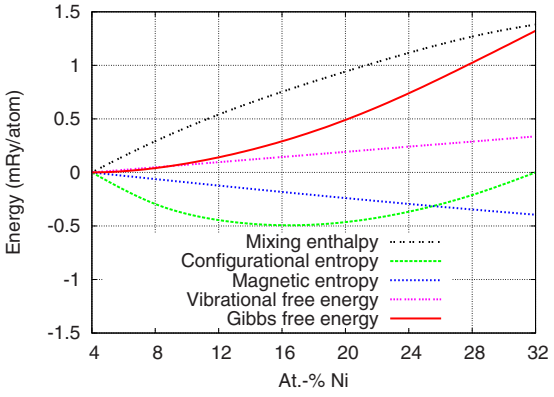

FIG. 3. (Color online) Calculated enthalpy and entropy contributions to the Gibbs free energy of formation for bcc $Fe_{0.84-n}Cr_{0.16}Ni_n$ plotted as a function of Ni content.

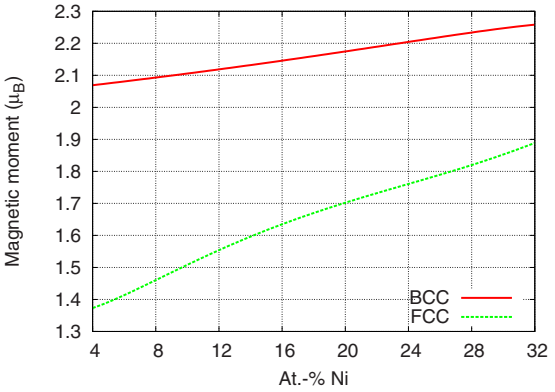

FIG. 4. (Color online) Local magnetic moment on Fe for fcc and bcc $Fe_{0.84-n}Cr_{0.16}Ni_n$ plotted as a function of Ni content.

particular, in low-Ni alloys we have $\mu_{Fe}^{bcc} - \mu_{Fe}^{fcc} \approx 0.7\mu_B$, which decreases to $\sim 0.4\mu_B$ in high-Ni alloys. Due to this difference, the magnetic entropy is always larger for the bcc phase compared to the fcc phase.

The trends from Fig. 4 can easily be understood if we take into account that in paramagnetic Fe-Cr-Ni alloys (described by the DLM state), Ni acts as a nonmagnetic spacer. With increasing Ni concentration, the interaction between magnetic Fe atoms decreases, which leads to bandwidth narrowing and ultimately to the increase in the Fe magnetic moments. However, due to structural differences, this effect is more pronounced for the close-packed fcc phase (coordination number 12) than for the more open bcc phase (coordination number 8), which explains the difference between the slopes for the fcc and bcc curves from the figure.

In contrast to the magnetic entropy, the vibrational free energy is calculated to stabilize the fcc phase (Figs. 2 and 3). Looking at the bulk moduli versus composition curves in Fig. 5, we observe that for all concentrations $B^{fcc} < B^{bcc}$, i.e., the fcc phase is softer compared to the bcc phase. Lower bulk modulus yields lower Debye temperature and larger phonon contribution to the Gibbs energy. The effect is more pronounced in low-Ni alloys and gradually decreases with increasing Ni content.

From the Gibbs free energy of formation for the bcc and fcc phases we find which phase is stable at a certain concentration. The Gibbs energy curves from Figs. 2 and 3 are

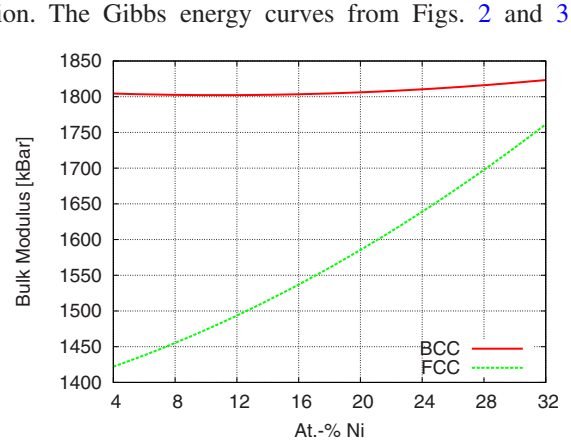

FIG. 5. (Color online) Bulk modulus for fcc and bcc $Fe_{0.84-n}Cr_{0.16}Ni_n$ plotted as a function of Ni content.

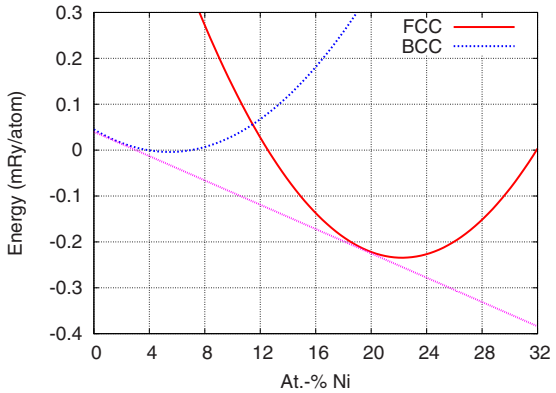

FIG. 6. (Color online) Gibbs free energies for bcc and fcc $Fe_{0.84-n}Cr_{0.16}Ni_n$ plotted as a function of Ni content. The duplex region corresponds to Ni concentrations ranging between the points where the Gibbs energies touch their common tangent.

compared to each other in Fig. 6. By drawing a common tangent to the fcc and bcc Gibbs energies, we find the concentration interval (2%–19% Ni), where the segregated system (duplex) is energetically more favorable than a single-phase alloy. Within this two-phase field region, the system breaks into Ni-enriched fcc and Ni-depleted bcc components. To the left/right of the duplex region the bcc/fcc phase is stable.

It is rather interesting to note that for both structures, the vibrational free-energy term is, to a large extent, canceled by the magnetic entropy term. Therefore, the actual shape of the Gibbs free energy of formation versus composition is mostly determined by the positive enthalpy of mixing plus the negative configurational entropy term. The almost perfect cancellation from Figs. 2 and 3, however, should be handled with precaution since for both the magnetic and the vibrational terms heavy approximations were used. In fact, as we will see it in Sec. III B, this cancellation is less efficient in low-Cr alloys. Nevertheless, the results from Figs. 4 and 5 are robust and indicate that, even with more advanced models for the magnetic and phonon contributions, there always will be a certain degree of cancellation between the above two terms.

We would like to emphasize that at static conditions, the $Fe_{1-c_0-n}Cr_{c_0}Ni_n$ quasibinary alloy always separates into a bcc $Fe_{1-c_0}Cr_{c_0}$ (containing eventually a small amount of Ni) alloy and a fcc $Fe_{0.68-c_0}Cr_{c_0}Ni_{0.32}$ alloy. This means that at low temperature, the width of the duplex region is strongly overestimated and temperature effects are crucial to recover the observed narrow two-phase field region between ferrite and austenite (see the TA1123 diagram[3]). Monitoring the mixing enthalpies from Figs. 2 and 3, we observe that for Ni-rich alloys the bcc-fcc energy difference is $\lesssim 1.4$ mRy/atom compared to $\lesssim 0.4$ mRy/atom obtained for the fcc-bcc energy difference for low-Ni alloys. This finding has important consequences. For instance, the (negative) configurational entropy has a more pronounced effect on the fcc stability field than on the bcc one. Assuming that the configurational entropy is the most significant temperature contribution for the phase diagram of paramagnetic Fe-Cr-Ni alloys (due to the aforementioned cancellation between the magnetic and vibrational terms), one can conclude that the increasing tem-

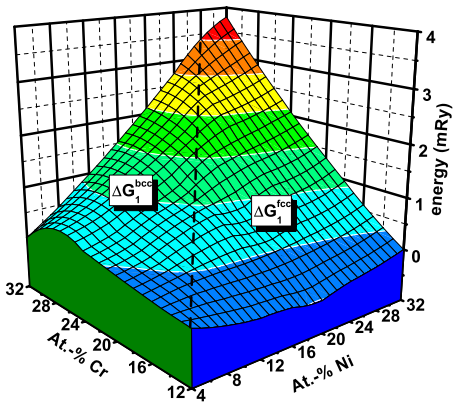

FIG. 7. (Color online) The Gibbs energy of formation without magnetic and vibrational entropy terms $[\Delta G_1^{\mathrm{str}}(c,n)]$ for $Fe_{1-c-n}Cr_cNi_n$ plotted as a function of Ni and Cr concentrations. Thick dashed line corresponds approximately to $\Delta G_1^{\mathrm{fcc}}(c,n) = \Delta G_1^{\mathrm{bcc}}(c,n)$.

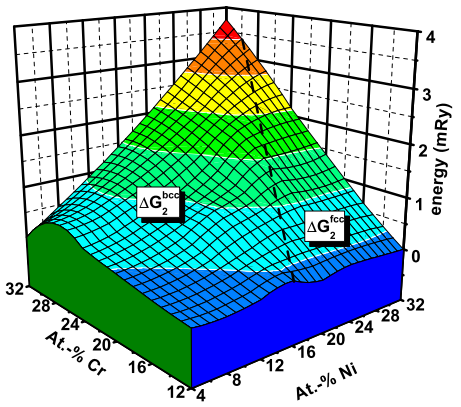

FIG. 8. (Color online) The Gibbs energy of formation without vibrational entropy term $[\Delta G_2^{\mathrm{str}}(c,n)]$ for $Fe_{1-c-n}Cr_cNi_n$ plotted as a function of Ni and Cr concentrations. Thick dashed line corresponds approximately to $\Delta G_2^{\mathrm{fcc}}(c,n) = \Delta G_2^{\mathrm{bcc}}(c,n)$.

perature will always broaden the austenite region faster than the ferrite region.

B. Theoretical phase diagram for paramagnetic Fe-Cr-Ni

The total energies with different Cr and Ni concentrations were calculated for fcc and bcc phases, and using the thermodynamic model described in Sec. II C, we constructed the Gibbs energies of formation and the stability fields for both structures. Since the Gibbs energy components are computed separately, in the following we will discuss the phase diagrams constructed at different levels of approximations.

In Fig. 7, we show the surface plot for the formation energy obtained merely from the enthalpy and configurational terms, viz., $\Delta G_1^{\mathrm{str}}(c,n) \equiv \Delta H^{\mathrm{str}}(c,n) - T\Delta S_{\mathrm{conf}}(c,n)$. Shown are $\Delta G_1^{\mathrm{bcc}}(c,n)$ for those concentrations where $\Delta G_1^{\mathrm{bcc}} < \Delta G_1^{\mathrm{fcc}}$ and $\Delta G_1^{\mathrm{fcc}}(c,n)$ for those concentrations where $\Delta G_1^{\mathrm{fcc}} < \Delta G_1^{\mathrm{bcc}}$. The thick dashed line corresponds approximately to the condition $\Delta G_1^{\mathrm{fcc}} = \Delta G_1^{\mathrm{bcc}}$. Using the common-tangent plane technique,[46] from Fig. 7 we can estimate the stability regions for the fcc and bcc phases. We find that the phase diagram (not shown) corresponding to this figure differs significantly from the TA1123 diagram.[3] There is a very narrow austenitic stability field in the low-Cr part of the map, and there are two small bcc regions located in the low-Cr and low-Ni and in the high-Cr and low-Ni corners.

The additional effect of the magnetic entropy is seen in Fig. 8. In this figure, we show the surface plot for the lowest $\Delta G_2^{\mathrm{str}}(c,n) \equiv \Delta H^{\mathrm{str}}(c,n) - T\Delta S_{\mathrm{conf}}(c,n) - T\Delta S_{\mathrm{mag}}^{\mathrm{str}}(c,n)$, i.e., $\Delta G_2^{\mathrm{bcc}}(c,n)$ on the left and $\Delta G_2^{\mathrm{fcc}}(c,n)$ on the right of the thick dashed line. With magnetic entropy included, the bcc region around the low-Cr and low-Ni corner is shifted toward higher Cr and Ni concentrations. In fact, we find that ΔG_2 yields a large ferrite region at the expense of the austenite region, which almost completely disappears from the map.

The surface plot constructed from the total Gibbs energy is given in Fig. 9. The conventions are the same as for the other two maps. Comparing Figs. 7–9, we find that, in line with our observations from Sec. III A, the vibrational free energy cancels, to some extent, the effect of the magnetic entropy. At the same time, the surface plot obtained from the total Gibbs energy shows some new features compared to that generated by G_1. First, in contrast to Figs. 7 and 8, the fcc Gibbs formation energy in Fig. 9 is a convex function for low-Cr alloys ($c \lesssim 0.2$) with a deep minimum around $c \approx 0.13-0.14$ and $n \approx 0.12-0.22$. Accordingly, the fcc stability field obtained from the total Gibbs energy is significantly larger than those obtained from ΔG_1 (or ΔG_2), and it extends toward the intermediate-Cr alloys. Another important feature of the surface plot from Fig. 9 is the concave $\Delta G^{\mathrm{bcc}}(c,n)$ for $n \lesssim 0.16$. In low-Ni alloys, this curve resembles the mixing enthalpy curve obtained for the paramagnetic bcc Fe-Cr alloys.[28] According to Fig. 9, the Ni-poor bcc alloys decompose into Cr-rich and Cr-poor alloys, limiting the bcc region to the low-Cr and low-Ni and to the high-Cr and low-Ni corners of the map. However, we should keep in mind that our results refer to completely random systems, neglecting the anomalous ordering effects present in ferritic Fe-Cr alloys.[44,47–49] These effects lower the formation energies of bcc alloys for intermediate-Cr concentration, stabilizing thus

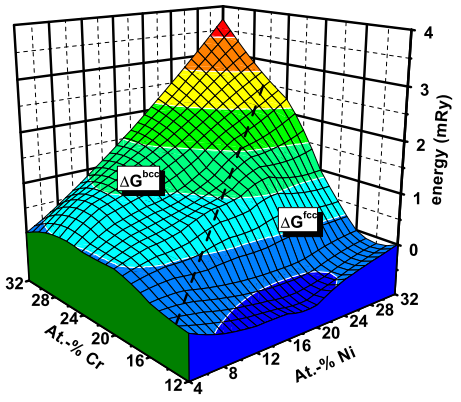

FIG. 9. (Color online) The Gibbs energy of formation $[\Delta G^{\mathrm{str}}(c,n)]$ for $Fe_{1-c-n}Cr_cNi_n$ plotted as a function of Ni and Cr concentrations. Thick dashed line corresponds approximately to $\Delta G^{\mathrm{fcc}}(c,n) = \Delta G^{\mathrm{bcc}}(c,n)$.

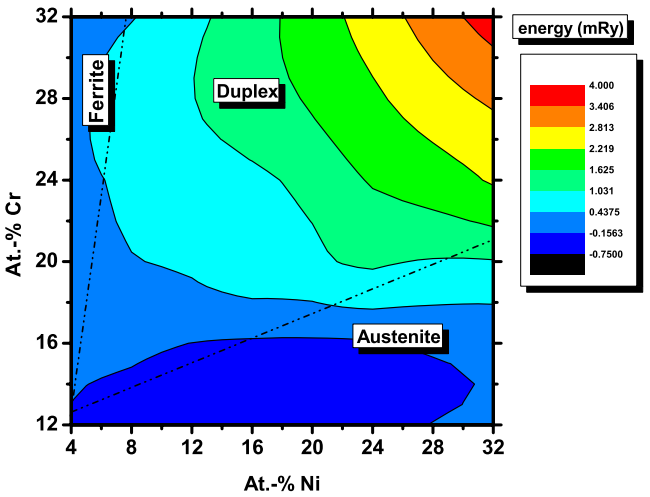

FIG. 10. (Color online) Theoretical high-temperature phase diagram for paramagnetic $Fe_{1-c-n}Cr_cNi_n$. For comparison, the contour plot for the minimal Gibbs energy of formation from Fig. 9 is also shown as a function of Ni and Cr concentrations. The two dashed lines mark the estimated ferrite-duplex and duplex-austenite boundaries.

a continuous ferrite field on the left-hand side of the map.

The theoretical high-temperature phase diagram for paramagnetic Fe-Cr-Ni alloys, constructed from the formation energies from Fig. 9, is shown in Fig. 10. The two dashed lines mark approximately the theoretical ferrite-duplex and duplex-austenite boundaries as derived using the common-tangent plane technique. We note that although the actual theoretical phase boundaries are not linear, here we approximate them by straight lines. In good agreement with the TA1123 diagram,[3] we find that the stability field for bcc is limited to low-Ni alloys ($n \lesssim 0.08$), there is a wide fcc stability field, and the width of the miscibility gap increases with alloying. On the other hand, our duplex field is shifted toward the high-Ni alloys, slightly underestimating the size of the austenite region. We speculate that this discrepancy may partly be due to the thermal spin fluctuations neglected in the present study. The average local magnetic moments are expected to decrease with temperature in Fe-rich bcc alloys,[43] whereas they show a marked increase in the fcc Fe-Cr-Ni alloys.[30,43] Therefore, the spin fluctuations should significantly alter the relative magnetic free energy, stabilizing the fcc phase relative to the bcc phase.

IV. CONCLUSIONS

Using the EMTO density-functional method in combination with the generalized-gradient approximation and the coherent-potential approximation, we have investigated the phase stability of paramagnetic Fe-Cr-Ni alloys. Comparing the Gibbs energies computed for the fcc and bcc phases as a function of chemical composition, we have identified the stability field of the two-phase duplex alloys. Taking into account the approximations made in the present study, the agreement between the present theoretical phase diagram and the one obtained from thermodynamic assessment[3] and experiments[15] can be considered satisfactory.

Comparing our result to the TA1123 diagram, we have found that the entropy contributions play a very important role in the formation of the duplex region. The magnetic entropy stabilizes the bcc phase, whereas the vibrational free energy always favors the soft fcc structure. These effects are mainly driven by the difference in bulk modulus and magnetic moment for the bcc and fcc structures. We mention that since these bulk parameters change in a monotonous manner (Figs. 4 and 5), any equation of state based on the data for the end points (reproducing correctly the value and the slope for B and μ_{Fe} for the bcc and fcc phases) would give very similar effects.

Due to the cancellation between vibrational and magnetic terms, the final phase diagram is to a large extent determined by the mixing enthalpy and the configurational entropy. At static conditions, the Fe-Cr-Ni system separates into Ni-depleted bcc and Ni-enriched fcc alloys, with strongly overestimated duplex region between the two phases. Our results show that the mixing enthalpy is smaller for the fcc phase than for the bcc phase, which means that the configurational entropy has a large broadening effect on the fcc region. Accordingly, the duplex region narrows and shifts toward the high-Cr alloys with increasing temperature.

The present study is an attempt to calculate the phase stability of paramagnetic duplex steels from *ab initio* theory. The results are promising and call for further improvements in the theoretical modeling of Fe-Cr-Ni alloys by accounting for all important factors for an accurate theoretical phase diagram as a function of temperature. Today, however, treating properly the anomalous magnetochemical effects in ferrites[44] or the magnetic and vibrational free energies in austenites, taking into account the large magnetoelastic effects in these alloys,[18,30] represents real challenges for modern computational material science.

ACKNOWLEDGMENTS

We wish to gratefully acknowledge the Academy of Finland (Research Grant No. 115362), COST (Action No. P19), and CSC, The Finnish IT center for Science, for their computational resources. Financial support from the Swedish Research Council, the Swedish Foundation for Strategic Research, and Hungarian Scientific Research Fund (Contract No. T048827) is also acknowledged.

*heikki.pitkanen@lut.fi

[1] J. Charles, *Proceedings of the Seventh Duplex 2007 International Conference & Expo*, Grado, Italy (AIM, Italy, 2007).

[2] P. Johansson and M. Liljas, *Proceedings of the Fourth European Stainless Steel Science and Market Congress* (Association Technique de la Siderurgie Francaise, Paris, France, 2002), Vol. 2, pp. 1–26.

[3] S. Hertzman and Bo Sundman, Scand. J. Metall. **14**, 95 (1985).

[4] S. Hertzman, P. J. Ferreira, and B. Brolund, Metall. Mater. Trans. A **28**, 277 (1997).

[5] S. Atamert and J. E. King, *Duplex Stainless Steels '91 International Conference* (Les Editions de Physique, Beaune, Bourgogne, France, 1991), p. 701.

[6] R. Mundt and H. Hoffmeister, *Stainless Steel '84 International Conference*, Gothenburg, Sweden (The Institute of Metals, London, 1984), p. 315.

[7] K. Ameyama, G. C. Weatherly, and K. T. Aust, Acta Metall. Mater. **40**, 1835 (1992).

[8] S. S. M. Tavaresa, R. F. de Noronha, M. R. da Silva, J. M. Neto, and S. Pairis, Mater. Res. **4**, 237 (2001).

[9] J. Cieslak, S. M. Dubiel, and B. Sepiol, J. Phys.: Condens. Matter **12**, 6709 (2000).

[10] A. K. Majumdar and P. v. Blanckenhagen, Phys. Rev. B **29**, 4079 (1984).

[11] M. J. Wozniak, A. Glowacka, and J. A. Kozubowski, J. Alloys Compd. **404-406**, 626 (2005).

[12] G. Wranglén, *An Introduction to Corrosion and Protection of Metals* (Chapman and Hall, New York, 1985).

[13] B. Sundman and J. Agren, J. Phys. Chem. Solids **42**, 297 (1981).

[14] M. Hillert and L.-I. Staffansson, Acta Chem. Scand. (1947-1973) **24**, 3618 (1970).

[15] T. Eriksson, Ph.D. thesis, Royal Institute of Technology, 1962.

[16] L. Vitos, *Computational Quantum Mechanics for Materials Engineers: The EMTO Method and Applications*, Engineering Materials and Processes Series (Springer-Verlag, London, 2007).

[17] J. Staunton, B. L. Gyorffy, A. J. Pindor, G. M. Stocks, and H. Winter, J. Magn. Magn. Mater. **45**, 15 (1984); B. L. Gyorffy, A. J. Pindor, J. Staunton, G. M. Stocks, and H. Winter, J. Phys. F: Met. Phys. **15**, 1337 (1985).

[18] L. Vitos, P. A. Korzhavyi, and B. Johansson, Phys. Rev. Lett. **96**, 117210 (2006).

[19] D. Music, T. Takahashi, L. Vitos, C. Asker, I. A. Abrikosov, and J. M. Schneider, Appl. Phys. Lett. **91**, 191904(3) (2007).

[20] M. van Schilfgaarde, I. A. Abrikosov, and B. Johansson, Nature (London) **400**, 46 (1999).

[21] P. Soven, Phys. Rev. **156**, 809 (1967); B. L. Gyorffy, Phys. Rev. B **5**, 2382 (1972).

[22] L. Vitos, I. A. Abrikosov, and B. Johansson, Phys. Rev. Lett. **87**, 156401 (2001).

[23] O. K. Andersen, O. Jepsen, and G. Krier, in *Lectures on Methods of Electronic Structure Calculations*, edited by V. Kumar, O. K. Andersen, and A. Mookerjee (World Scientific, Singapore, 1994), p. 63.

[24] O. K. Andersen, C. Arcangeli, R. W. Tank, T. Saha-Dasgupta, G. Krier, O. Jepsen, and I. Dasgupta, in *Tight-Binding Approach to Computational Materials Science*, edited by P. E. A. Turchi, A. Gonis, and L. Colombo, MRS Symposia Proceedings No. 491 (Materials Research Society, Pittsburgh, 1998), pp. 3–34.

[25] L. Vitos, Phys. Rev. B **64**, 014107 (2001).

[26] L. Vitos, H. L. Skriver, B. Johansson, and J. Kollár, Comput. Mater. Sci. **18**, 24 (2000).

[27] L. Vitos, P. A. Korzhavyi, and B. Johansson, Phys. Rev. Lett. **88**, 155501 (2002); Nature Mater. **2**, 25 (2003).

[28] P. Olsson, I. A. Abrikosov, L. Vitos, and J. Wallenius, J. Nucl. Mater. **321**, 84 (2003).

[29] L. Dubrovinsky, N. Dubrovinskaia, F. Langenhorst, D. Dobson, D. Rubie, C. Gesmann, I. Abrikosov, V. I. Baykov, L. Vitos, B. Johansson, T. Le Bihan, and Wilson A. Crichton, Nature (London) **422**, 58 (2003).

[30] L. Vitos and B. Johansson, Phys. Rev. B **79**, 024415 (2009).

[31] N. Dubrovinskaia, L. Dubrovinsky, I. Kantor, W. A. Crichton, V. Dmitriev, V. Prakapenka, G. Shen, L. Vitos, R. Ahuja, B. Johansson, and I. A. Abrikosov, Phys. Rev. Lett. **95**, 245502 (2005).

[32] A. Taga, L. Vitos, B. Johansson, and G. Grimvall, Phys. Rev. B **71**, 014201 (2005).

[33] L. Huang, L. Vitos, S. K. Kwon, B. Johansson, and R. Ahuja, Phys. Rev. B **73**, 104203 (2006).

[34] J. Zander, R. Sandström, and L. Vitos, Comput. Mater. Sci. **41**, 86 (2007).

[35] A. E. Kissavos, S. I. Simak, P. Olsson, L. Vitos, and I. A. Abrikosov, Comput. Mater. Sci. **35**, 1 (2006).

[36] B. Magyari-Köpe, G. Grimvall, and L. Vitos, Phys. Rev. B **66**, 064210 (2002).

[37] B. Magyari-Köpe, L. Vitos, and G. Grimvall, Phys. Rev. B **70**, 052102 (2004).

[38] B. Magyari-Köpe, L. Vitos, B. Johansson, and J. Kollár, Acta Crystallogr., Sect. B: Struct. Sci. **57**, 491 (2001).

[39] B. Magyari-Köpe, L. Vitos, B. Johansson, and J. Kollár, J. Geophys. Res. **107**, 2136 (2002).

[40] A. Landa, C.-C. Chang, P. N. Kumta, L. Vitos, and I. A. Abrikosov, Solid State Ionics **149**, 209 (2002).

[41] B. Magyari-Köpe, L. Vitos, G. Grimvall, B. Johansson, and J. Kollár, Phys. Rev. B **65**, 193107 (2002).

[42] J. P. Perdew, K. Burke, and M. Ernzerhof, Phys. Rev. Lett. **77**, 3865 (1996).

[43] A. V. Ruban, S. Khmelevskyi, P. Mohn, and B. Johansson, Phys. Rev. B **75**, 054402 (2007).

[44] A. V. Ruban, P. A. Korzhavyi, and B. Johansson, Phys. Rev. B **77**, 094436 (2008).

[45] P. Söderlind, L. Nordström, Lou Yongming, and B. Johansson, Phys. Rev. B **42**, 4544 (1990).

[46] M. Hillert, *Phase Equilibria, Phase Diagrams and Phase Transformations* (Cambridge University Press, Cambridge, 2008).

[47] T. P. C. Klaver, R. Drautz, and M. W. Finnis, Phys. Rev. B **74**, 094435 (2006).

[48] P. Olsson, I. A. Abrikosov, and J. Wallenius, Phys. Rev. B **73**, 104416 (2006).

[49] P. Olsson, C. Domain, and J. Wallenius, Phys. Rev. B **75**, 014110 (2007).